Late-time power-law tails of free atomic spontaneous emission

Tasuku Ono
Physics Department and Center for Ultracold Atoms,
Massachusetts Institute of Technology, Cambridge, MA 02139, USA
(Dated: May 26, 2026)

Atomic spontaneous emission is one of the most fundamental processes in atomic physics. The textbook exponential law is, however, only an intermediate-time approximation: at sufficiently long times, the survival probability decays as a power law set by the threshold behavior of the spectral density. Within a single-channel rotating-wave model and a specified Coulomb-gauge bare excited-state projector, we derive late-time laws $P(t) \sim t^{-2p}$ for pure one-photon atomic multipole transitions in free space, with the exponent p determined by the model threshold power. We further obtain a closed-form envelope estimate for the crossover time t_x under a long-wavelength monomial-form-factor approximation, giving $t_x/\tau \sim 2(p+1)\ln Q$ for the quality factor $Q \gg 1$, where τ is the lifetime. Applied to four representative transitions with distinct multipole character, the estimate gives a transparent model ranking: broad electric-dipole lines reach the asymptotic regime soonest in units of lifetime, although the free-space tail remains experimentally inaccessible.

Introduction.— The spontaneous emission of light by an excited atom is among the most fundamental processes in quantum mechanics. Einstein's identification of the A coefficient [1] and the subsequent derivation by Weisskopf and Wigner [2] established the textbook picture that an isolated excited state $|e\rangle$ decays exponentially as $P_e(t) = e^{-\Gamma t}$, with Γ given by Fermi's golden rule. This result is central to laser physics, atomic line shapes, atomic clocks, and the modern understanding of light–matter interaction [3].

The exponential law, however, is an approximation that fails at sufficiently long times. As proved by Khalfin [4] and developed in detail by Fonda, Ghirardi, and Rimini [5], the requirement that the Hamiltonian be bounded from below forces the survival probability to decay slower than any exponential at late times, with a power-law tail $P_e(t) \propto t^{-\alpha}$ set by the analytic structure of the spectral density. These foundational considerations remain a subject of active investigation: signatures of non-exponential decay have been observed in tunneling systems [6, 7], in molecular luminescence [8], and most recently in integrated photonic simulators that resolved the full short-time/exponential/long-time sequence [9]. At the same time, theoretical work continues to refine the gauge structure [10–13] and the multichannel generalization [14] of the older frameworks.

Yet despite this sustained activity, in the free-space atomic setting specifically, the question has been approached in a curiously fragmented way. Theoretically, Facchi and Pascazio [15] analytically established $P_e(t) \sim t^{-4}$ for the hydrogen $2\mathrm{P} \to 1\mathrm{S}$ transition, and Giacosa and Kyzioł [16] numerically located the exponential-to-power-law crossover at $t_x \approx 125$ times its lifetime for the same transition. For higher multipoles, Lassalle *et al.* [17] computed the multipole-resolved coupling spectrum but applied it to the monitored anti-Zeno problem. Experimentally, the power-law tail has been seen in the non-atomic platforms as noted above, but not in free-space spontaneous emission of an atomic line due to practical limitations. What is still useful, especially pedagogically, is a compact synthesis of the standard threshold-law argument with the multipole-resolved free-space spectra in the simplest possible setting—an atom radiating into the free-space photon vacuum.

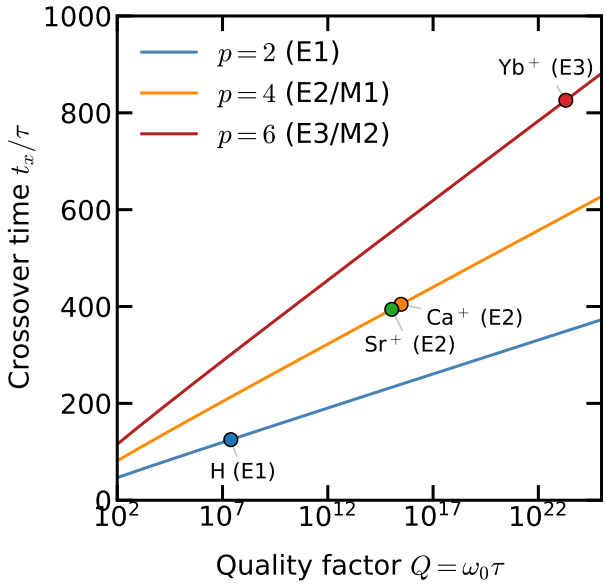

FIG. 1. Envelope exponential-to-power-law turnover time t_x/τ as a function of the quality factor $Q = \omega_0\tau$, where ω_0 is the atomic transition frequency and $\tau = 1/\Gamma$ is the lifetime. The solid curves show the asymptotic estimate used in these notes, where p is the multipole exponent of the late-time tail. Markers indicate the real transitions of Table I. EL (ML) indicates the electric (magnetic) character of the transition with multipole order L.

To this end, we carry out the analysis of a gauge-fixed bare-state survival amplitude for atomic spontaneous emission in free space at late times. Our results are threefold. First, using the Coulomb-gauge spectrum, we

derive the explicit late-time survival laws $P_{EL}(t) \sim t^{-4L}$ and $P_{ML}(t) \sim t^{-(4L+4)}$ for electric (E) and magnetic (M) transitions of multipole order L, giving the ranking $E_1 > E_2 \sim M_1 > E_3 \sim M_2 > \cdots$ for the onset of the power-law tail within this convention. These multipole tail laws are a direct consequence of ingredients available in the literature; here we collect them in closed form and connect them to the unmonitored survival problem. Second, we obtain an analytical envelope estimate for the exponential-to-power-law crossover time t_x as a function of the transition frequency ω_0, the intermediate-time exponential decay rate Γ and the multipole exponent p, with asymptotic scaling $t_x/\tau \sim 2(p+1)\ln Q$, where $Q = \omega_0/\Gamma$. Finally, we quantify the observability of the power-law tail by applying this formula to four representative atomic transitions with distinct multipoles spanning about sixteen orders of magnitude in Q. For the sake of these notes, the remainder of the discussion is organized in a careful, pedagogical sequence: we review the Coulomb-gauge derivation of exponential decay, identify the breakdown mechanism at long times, and address the gauge sensitivity of the off-shell survival amplitude.

Spontaneous emission of an atom.— Our system is a single atomic excited state coupled to the vacuum photon continuum, one of the simplest settings available in atomic physics. The atom-field Hamiltonian is

$$H = H_A + H_F + V, \tag{1}$$

where $H_A = E_e\,|e\rangle\langle e| + E_g\,|g\rangle\langle g|$ is the bare atom Hamiltonian with excited state $|e\rangle$ and ground state $|g\rangle$, and $H_F = \sum_{k,\lambda} \hbar\omega_k a^\dagger_{k\lambda} a_{k\lambda}$ is the free-field Hamiltonian with wavenumber k and polarization λ. We work in the Coulomb gauge, where the vector potential satisfies $\nabla\cdot\mathbf{A} = 0$ and the interaction retained here is the linear minimal-coupling term

$$V = \frac{e}{m_e}\,\hat{\mathbf{A}}(\mathbf{0})\cdot\hat{\mathbf{p}}, \tag{2}$$

shown first in its electric-dipole form. For the higher-multipole threshold laws derived below, the full spatial factor $e^{i\mathbf{k}\cdot\mathbf{r}}$ is retained before taking the long-wavelength expansion, as described in Appendix C. The A^2 term and counter-rotating terms are outside the one-photon rotating-wave model used for the main estimates; this is one reason the off-shell tail should be read as a model/projector-dependent quantity rather than a fully gauge-invariant QED prediction. The quantized vector potential is written with e denoting the positive elementary charge; the overall sign is immaterial for the decay rate:

$$\hat{\mathbf{A}}(\mathbf{0}) = \sum_{k,\lambda} \mathcal{A}_k\,\boldsymbol{\epsilon}_{k\lambda}\left(a_{k\lambda} + a^\dagger_{k\lambda}\right), \qquad \mathcal{A}_k = \sqrt{\frac{\hbar}{2\epsilon_0\omega_k V}}.$$

Note that $\mathcal{A}_k \propto \omega_k^{-1/2}$, in contrast to the electric-field amplitude $\mathcal{E}_k \propto \omega_k^{+1/2}$ appearing in the length-gauge formulation $V = -\mathbf{d}\cdot\mathbf{E}$ (Appendix A). This difference is inconsequential on shell at $\omega = \omega_0 \equiv (E_e - E_g)/\hbar$ but changes the low-frequency threshold behavior of the spectral density and hence the late-time power-law tail of the decay curve. Although not the central theme of these notes, we revisit this discrepancy later. Under the rotating-wave approximation, the coupling (2) becomes

$$V = \hbar\sum_{k,\lambda}\left[g_{k\lambda}\,a^\dagger_{k\lambda}\sigma_- + g^*_{k\lambda}\,a_{k\lambda}\sigma_+\right], \tag{3}$$

where $\sigma_- = |g\rangle\langle e|$, $\sigma_+ = |e\rangle\langle g|$, and the coupling constant is

$$\hbar g_{k\lambda} = \frac{e}{m_e}\,\mathcal{A}_k\,\boldsymbol{\epsilon}_{k\lambda}\cdot\mathbf{p}_{ge}, \qquad \mathbf{p}_{ge} = \langle g|\hat{\mathbf{p}}|e\rangle. \tag{4}$$

The model survival measurement begins by preparing the gauge-fixed bare state $|\psi(0)\rangle = |e;0\rangle$ and later projecting back onto the same state. Under the atom-field coupling (3), the state evolves to

$$|\psi(t)\rangle = c_e(t)e^{-iE_e t/\hbar}|e;0\rangle + \sum_{k,\lambda} c_{k\lambda}(t)e^{-i(E_g+\hbar\omega_k)t/\hbar}|g;1_{k\lambda}\rangle.$$

Eliminating the photon amplitudes gives an exact equation for the excited-state amplitude:

$$\dot{c}_e(t) = -\int_0^t dt'\,K(t-t')c_e(t'), \tag{5}$$

with $K(\tau) = \sum_{k,\lambda}|g_{k\lambda}|^2 e^{-i(\omega_k-\omega_0)\tau}$. For a detailed derivation, see Appendix B.

An important step here is the continuum approximation. Physically, the emitted photon can occupy an enormous number of free-space modes whose frequencies are so closely spaced that the mode sum is effectively smooth. In this case the kernel is replaced by

$$K(\tau) = \int_0^\infty d\omega\,J(\omega)e^{-i(\omega-\omega_0)\tau}, \tag{6}$$

where the spectral density is

$$J(\omega) = \sum_\lambda \rho_\lambda(\omega)\,|g_\lambda(\omega)|^2, \tag{7}$$

with $\rho_\lambda(\omega)$ the photon density of states.

Having established the framework, we derive the conventional exponential decay of an excited atom. In the weak-coupling regime, the continuum loses phase memory much faster than the atom decays. In the memory integral (5), this means that $c_e(t')$ changes little over the time for which $K(t-t')$ is appreciable, so the history dependence can be replaced by the instantaneous amplitude $c_e(t)$. The remaining time integral of $K(\tau)$ then selects the near-resonant part of $J(\omega)$: modes with $\omega \neq \omega_0$ acquire rapidly varying phases $e^{-i(\omega-\omega_0)\tau}$ and cancel, while modes near ω_0 add coherently. This gives the familiar Fermi-golden-rule rate

$$\Gamma = 2\pi J(\omega_0). \tag{8}$$

The off-resonant part of the continuum does not cause irreversible loss but shifts the phase of the excited state by a small amount Δ. Thus the nonlocal equation reduces to the local amplitude equation

$$\dot{c}_e(t) = -\left(\frac{\Gamma}{2} + i\Delta\right) c_e(t), \tag{9}$$

yielding the familiar exponential survival probability $P_e(t) = |c_e(t)|^2 = e^{-\Gamma t}$.

Power-law decay at late times.— Going to the late-time regime prompts us to focus on the feature of the continuum at low frequency. Indeed, the integral in (6) starts at $\omega = 0$, so the atom–photon continuum has lowest energy $E_{\rm th} = E_g$, around which $J(\omega)$ follows some scaling with ω. This lower edge is far from resonance, so it is irrelevant for the initial exponential decay. At very long times, however, Fourier transforms are sensitive to endpoints, i.e., the phase $\omega\tau$ starts to pick up non-negligible contributions from ω near the threshold. The excited-state amplitude therefore has two qualitatively different pieces, $c_e(t) = c_{\rm exp}(t) + c_{\rm cut}(t)$, where $c_{\rm exp}(t)$ is the previously obtained solution of Eq. (9) from the near-resonance spectrum, and $c_{\rm cut}(t)$ comes from the lower endpoint of the same continuum. Near this endpoint, the photon frequency is $\omega = \epsilon/\hbar$, where $\epsilon = E - E_{\rm th}$ is some small energy scale compared to the inverse of the ordinary (early) decay time. At the level of the exponent, and up to a smooth prefactor that does not change the power law, the threshold contribution is controlled by $J(\epsilon/\hbar)$:

$$c_{\rm cut}(t) \propto e^{-i(E_{\rm th}-E_e)t/\hbar} \int_0^\infty d\epsilon\, J(\epsilon/\hbar)\, e^{-i\epsilon t/\hbar}. \tag{10}$$

Note that the integral can be extended to infinity because the high-frequency part is averaged away, except at the resonance which is already accounted for in $c_{\rm exp}$. A perfect exponential decay would require a spectral function extending to $\omega = -\infty$, which is forbidden by the lower bound $\omega \geq 0$. Conversely, the non-exponential contribution at late times comes from the lower endpoint of the continuum [4, 5].

Having identified the contribution from the low-frequency component of the continuum, we can now ask how the late-time tail depends on it. Assume the spectral density has a power-law threshold scaling $J(\omega) \sim \omega^s$ as $\omega \to 0^+$, with $s > -1$ and with a smooth nonzero coefficient near the threshold, no threshold bound-state pole, and no stronger singularity at the endpoint. Then (10) gives, at late times,

$$\begin{aligned} c_{\rm cut}(t) &\sim e^{-i(E_{\rm th}-E_e)t/\hbar} \int_0^\infty d\epsilon\, \epsilon^s\, e^{-i\epsilon t/\hbar} \\ &= \Gamma_{\rm Eul}(s+1)\, e^{-i\pi(s+1)/2} \left(\frac{\hbar}{t}\right)^{s+1} e^{-i(E_{\rm th}-E_e)t/\hbar}, \end{aligned}$$

where $\Gamma_{\rm Eul}$ is Euler's gamma function, so that

$$P_e(t) \;\sim\; t^{-2(s+1)}. \tag{11}$$

In summary, the same spectral density $J(\omega)$ controls two different regimes: its value at the resonance, $J(\omega_0)$, sets the ordinary exponential lifetime, while its small-ω power sets the late-time, *power-law* tail.

Multipole structure of the late-time tail.— The relationship between the low-frequency behavior of the spectral density and the late-time tail can be applied to an atom in free space after specifying the model and projector. We use the known coupling spectrum for a pure one-photon transition in free space in the Coulomb gauge [17–19] (see Appendix C for the derivation),

$$\rho(\omega) \propto \omega^2, \;\; |g_{EL}(\omega)|^2 \propto \omega^{2L-3}, \;\; |g_{ML}(\omega)|^2 \propto \omega^{2L-1}, \tag{12}$$

where g_{EL} and g_{ML} are the electric and magnetic multipole couplings, respectively, and L is the multipole order. For example, the $L = 1$ electric case is just the $\mathcal{A}_k^2 \propto \omega^{-1}$ behavior of the vector potential; each higher electric multipole adds the long-wavelength factor $(kr)^2 \propto \omega^2$ to $|g|^2$, while the magnetic multipole of order L carries one additional power of kr relative to the corresponding electric multipole. The resulting spectral densities are

$$J_{EL}(\omega) \propto \omega^{2L-1}, \qquad J_{ML}(\omega) \propto \omega^{2L+1} \qquad (\omega \to 0^+). \tag{13}$$

It is useful to define the late-time amplitude exponent $p \equiv s+1$, so that $P_e(t) \sim t^{-2p}$. Combining (11) and (13) gives $p_{EL} = 2L$ and $p_{ML} = 2L + 2$, or equivalently

$$P_{EL}(t) \sim t^{-4L}, \qquad P_{ML}(t) \sim t^{-(4L+4)}. \tag{14}$$

Within this Coulomb-gauge bare-projector model, the threshold physics therefore ranks the free-decay tails:

$$E_1 \;>\; E_2 \sim M_1 \;>\; E_3 \sim M_2 \;>\; \cdots, \tag{15}$$

where ">" means an earlier and less strongly suppressed post-exponential envelope. Note that the multipole-resolved threshold exponents behind (13) appear in Lassalle *et al.* [17] in the context of the (monitored) anti-Zeno effect. However, their consequence for the free, unmonitored survival probability at late times is useful to collect explicitly [20].

As a coherence check, consider the hydrogen $2\mathrm{P} \to 1\mathrm{S}$ line, which is an electric-dipole transition with $L = 1$. Our formula (14) gives $P_e(t) \sim t^{-4}$, in agreement with the analytic result of Facchi and Pascazio [15] and the numerical computation of Giacosa and Kyzioł [16].

With the relation of the late-time tail to the low-frequency threshold behavior of the spectral density established, we now revisit the gauge convention. The threshold exponent derived above is a statement about the Coulomb-gauge, $\mathbf{A}\cdot\mathbf{p}$, description used in the hydrogenic form factor of Eq. (12). This convention matters for late-time tails because the tail samples the off-resonant, low-frequency part of $J(\omega)$, not only the value at ω_0. In the length-gauge interaction $V = -\mathbf{d}\cdot\mathbf{E}$ of Power and Zienau [21, 22], the electric-field amplitude scales as $\mathcal{E}_k \propto \omega_k^{1/2}$ rather than $\mathcal{A}_k \propto \omega_k^{-1/2}$, shifting the

low-frequency power of an electric-dipole spectral density from $J(\omega) \propto \omega$ to $J(\omega) \propto \omega^3$, the familiar free-space electric-dipole scaling. More generally, the usual multipolar radiation scaling would give

$$J_{EL}^{(\mathrm{mult})}(\omega) \sim J_{ML}^{(\mathrm{mult})}(\omega) \sim \omega^{2L+1}, \qquad P_e(t) \sim t^{-(4L+4)}. \tag{16}$$

Hence, for an electric dipole the corresponding tail changes from $P_e(t) \sim t^{-4}$ to $P_e(t) \sim t^{-8}$.

The apparent discrepancy between gauge choices does not contradict gauge invariance of physical observables. On shell, $\langle g|\hat{\mathbf{p}}|e\rangle = im_e\omega_0\langle g|\hat{\mathbf{r}}|e\rangle$ at $\omega = \omega_0$, so the Fermi-golden-rule rate $\Gamma = 2\pi J(\omega_0)$ is the same. The late-time survival amplitude, however, is an off-shell property of a chosen bare excited state, and that state is itself gauge-sensitive: the bare excited state $|e\rangle \otimes |0\rangle$ refers to physically distinct dressed configurations in the two gauges, related by the unitary transformation [3, 21, 22]. For the sake of these notes, it is useful to briefly recall the history of this problem. The issue was first raised by Lamb [23, 24], who argued on spectroscopic grounds that the multipolar/length gauge provides the operationally correct projection onto atomic eigenstates. The specific gauge sensitivity of the spontaneous-emission tail was discussed by Knight and Milonni [25] and later developed by Seke [19] and Enaki [26]. Aharonov and Au [27] pointed out that the two gauges answer slightly different physical questions about the dressing of the unstable state and are therefore both internally consistent within their own definitions of the bare atom. A more modern resolution, provided by Vukics, Kónya, and Domokos [10] is that both pictures derive from the same gauge-invariant Lagrangian, with the apparent disagreement reflecting different choices of canonical variables rather than a physical inconsistency. Direct numerical comparison of the two gauges for the hydrogen $2\mathrm{P} \to 1\mathrm{S}$ problem [28] finds agreement at a high accuracy throughout the exponential regime. The late-time gauge dependence sits well below this numerical floor and is at present beyond experimental reach. Thus the detailed equivalence classes in Eq. (15) should not be read as gauge-invariant observables: in the multipolar scaling one instead has $E_1 \sim M_1 > E_2 \sim M_2 > E_3 \sim M_3 > \cdots$. What is robust in this model comparison is the qualitative statement that lower threshold powers produce earlier and slower tails. In what follows we keep the Coulomb-gauge convention because it is the convention used in the hydrogen benchmark and in the free-space form factors from which (13) was derived.

Turnover estimate and applications to real atomic transitions.— Within the specified single-channel model, observability of the late-time decay depends on when it overtakes the exponential. To estimate the crossover from the exponential to the power-law, we need the absolute magnitude of $c_{\mathrm{cut}}(t)$, not only its t-dependence. To this end, the smooth prefactor absorbed into "$\propto$" in (10) must now be made explicit. The fastest way to estimate the prefactor is to realize that in the memory integral (6), off-resonant modes at frequency ω accumulate a phase $e^{-i(\omega-\omega_0)\tau}$. In the frequency-domain form of the memory equation this produces two off-resonant propagators, as derived in Appendix D, so the full threshold amplitude carries an energy denominator $(\omega-\omega_0)^{-2}$:

$$c_{\mathrm{cut}}(t) \;\sim\; e^{-i(E_{\mathrm{th}}-E_e)t/\hbar}\int_0^\infty d\omega\,\frac{J(\omega)}{(\omega-\omega_0)^2}\,e^{-i\omega t}. \tag{17}$$

At the threshold $\omega \to 0^+$, this gives a prefactor ω_0^{-2}. Writing the low-frequency spectral density as $J(\omega) \simeq C_J\,\omega^{p-1}$ and applying the asymptotic evaluation of Eq. (11) gives

$$|c_{\mathrm{cut}}(t)| \;\simeq\; \frac{C_J\,\Gamma_{\mathrm{Eul}}(p)}{\omega_0^2}\,t^{-p}, \tag{18}$$

To connect the threshold coefficient to the measured linewidth, we make a long-wavelength monomial-form-factor approximation,

$$\begin{aligned} J(\omega) &\simeq J(\omega_0)\left(\frac{\omega}{\omega_0}\right)^{p-1}F(\omega), \\ F(\omega_0) &= 1, \qquad F(0) \simeq 1. \end{aligned} \tag{19}$$

Equivalently, since $\Gamma = 2\pi J(\omega_0) \simeq 2\pi C_J\omega_0^{p-1}$ in this approximation, one has $C_J \simeq \Gamma/(2\pi\omega_0^{p-1})$. Substituting back into (18), we obtain the leading envelope amplitude estimate in terms of line parameters:

$$|c_{\mathrm{cut}}(t)| \;\simeq\; \frac{\Gamma_{\mathrm{Eul}}(p)\,\Gamma}{2\pi\,\omega_0^{p+1}}\,t^{-p}. \tag{20}$$

We define t_x operationally as the envelope crossover $|c_{\mathrm{exp}}(t_x)| = |c_{\mathrm{cut}}(t_x)|$. This ignores the oscillatory interference term in $|c_{\mathrm{exp}} + c_{\mathrm{cut}}|^2$, so it should not be read as a unique observable transition time. The definition gives

$$t_x = -\frac{2p}{\Gamma}\,W_{-1}\left[-\frac{\Gamma}{2p}\left(\frac{\Gamma_{\mathrm{Eul}}(p)\,\Gamma}{2\pi\,\omega_0^{p+1}}\right)^{1/p}\right], \tag{21}$$

where W_{-1} is the negative branch of the Lambert function [29]. For a large quality factor $Q = \omega_0/\Gamma \gg 1$, the asymptotic behavior of W_{-1} gives

$$\frac{t_x}{\tau} \;\sim\; 2(p+1)\ln Q, \qquad \tau = \Gamma^{-1}. \tag{22}$$

In this envelope definition, broad low-multipole lines are favored, while narrow forbidden lines are disfavored both because they have larger p and because they have much larger Q.

The turnover formula provides an envelope estimate of the observability of the late-time tail for an idealized pure single-channel atomic transition. Here, we consider four representative transitions spanning about sixteen orders of magnitude in Q and three multipole orders: the

TABLE I. Late-time-tail observability for representative atomic transitions. Computed in the Coulomb gauge from Eq. (21). The quality factor $Q = \omega_0\tau$, the multipole exponent p, and the crossover time t_x are reported both in units of the lifetime and in absolute units. The final column gives the envelope population $P_x \equiv e^{-t_x/\tau}$ at crossover.

Transition	L, type	p	$Q=\omega_0\tau$	t_x/τ	t_x	$\log_{10} P_x$
H $2P\to1S$	1, E1	2	2.5×10^{7}	125	200 ns	−54
Ca^+ $D_{5/2}$	2, E2	4	3.0×10^{15}	405	473 s	−176
Sr^+ $D_{5/2}$	2, E2	4	1.1×10^{15}	394	154 s	−171
$^{171}Yb^+$ $F_{7/2}$	3, E3	6	2.0×10^{23}	826	1.3×10^{3} yr	−359

hydrogen $2P\to1S$ Lyman-α line (E1, $\lambda = 121.6$ nm, $\tau = 1.595$ ns), the electric-quadrupole clock lines of Ca^+ ($3D_{5/2}\to4S_{1/2}$, $\lambda = 729$ nm, $\tau = 1.168$ s) [30] and Sr^+ ($4D_{5/2}\to5S_{1/2}$, $\lambda = 674$ nm, $\tau = 390.8$ ms) [31], and the electric-octupole clock transition of $^{171}Yb^+$ ($2F_{7/2}\to 2S_{1/2}$, $\lambda = 467$ nm, $\tau \approx 1.58$ yr) [32]. Table I collects the computed quantities. These entries should be read as pure-channel idealizations. If several radiative channels contribute, $J_{\rm tot}(\omega) = \sum_i J_i(\omega)$, the asymptotic tail is set by the smallest threshold power among channels with nonzero coupling, even when that channel has a small branching ratio.

Figure 1 plots t_x/τ as a function of Q for the three relevant multipole exponents $p = 2, 4, 6$, with the four representative transitions overlaid. Two features deserve emphasis. First, the $\log Q$ growth is mild: even when Q varies by sixteen orders of magnitude, t_x/τ varies only by a factor of about seven. The dominant ranking is thus set by the multipole exponent p through the prefactor $2(p+1)$, not by Q. Second, forbidden clock lines pay a double penalty: a larger p pushes the crossover later in units of the lifetime, and a vastly larger τ makes the absolute crossover time astronomically large. For the $^{171}Yb^+$ octupole clock, the post-exponential regime begins only after roughly 10^3 years of evolution.

These numbers also clarify what "observability" can and cannot mean. Figure 2 shows the explicit hydrogen survival probability. By the time t_x is reached, the surviving population is of order 10^{-54}, exponentially suppressed by the preceding ∼125 lifetimes of ordinary decay, as also pointed out in [16]. Detecting the post-exponential tail of a single isolated atomic line in free space is therefore not a near-term experimental program. What our ranking identifies is not which line could realistically be observed, but which line reaches its asymptotic regime soonest in units of its lifetime. The natural place to look for these tails remains structured photonic reservoirs and other engineered systems [9], where the threshold can be brought close to ω_0 and the survival probability at t_x is no longer exponentially small. Nevertheless, the free-space calculation specifies the threshold powers of the corresponding pure multipole channels before any reservoir engineering is added.

Conclusion and outlook.— In these notes, we have

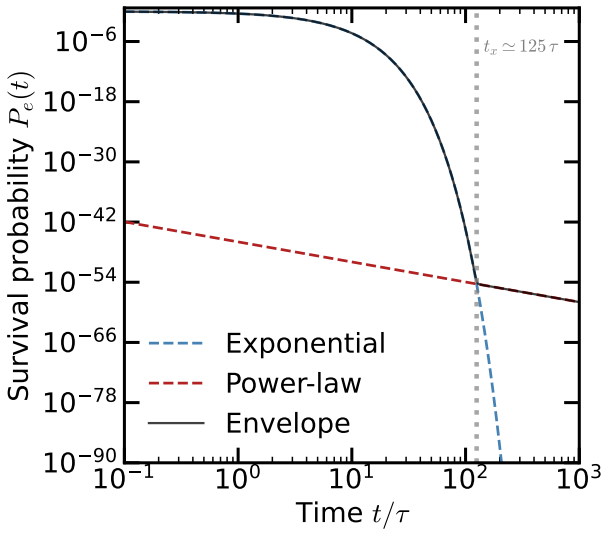

FIG. 2. Envelope survival probability for the hydrogen $2P\to1S$ line. The exponential part $|c_{\rm exp}|^2 \propto e^{-t/\tau}$ (blue) dominates until $t\approx125\,\tau$. After that, the power-law envelope $|c_{\rm cut}|^2 \propto t^{-4}$ (red) takes over. By the envelope crossover the survival population is already $\sim 10^{-54}$ of the original population.

derived the explicit late-time power-law decay of a gauge-fixed bare excited state in a single-channel Coulomb-gauge model of free-space spontaneous emission, $P_{EL}(t) \sim t^{-4L}$ and $P_{ML}(t) \sim t^{-(4L+4)}$ for a pure atomic multipole transition. Using the same framework, and the monomial-form-factor approximation in Eq. (19), we also obtained a closed-form envelope estimate for the exponential-to-power-law crossover time $t_x(\omega_0, \Gamma, p)$ that reduces to $t_x/\tau \sim 2(p+1)\ln Q$ in the high-Q limit. We further applied it to four representative transitions spanning about sixteen orders of magnitude in quality factor. The central physical lesson is that late-time deviations from the usual exponential decay are controlled by the low-frequency threshold behavior of the spectral density, while the ordinary lifetime is controlled by the on-shell value of the same spectral density. Broad electric-dipole transitions minimize the model envelope crossover in units of lifetime, but even the best free-space case remains experimentally inaccessible because the surviving population is already exponentially tiny.

Three extensions are natural. First, engineering a cavity around an atom to manipulate the spectrum can change the decay profile. The trivial case is a lossy single-mode cavity resonant with the atomic transition. In this case, spontaneous emission is enhanced at the resonance and the late-time tail at low frequencies becomes more difficult to see. The other extreme is when the resonant decay is suppressed or the relevant thresh-

old is brought close to the transition, in which case the envelope crossover time can be shortened. Second, hyperfine mixing can shorten an otherwise forbidden ultranarrow E3 or M2 lifetime by an order of magnitude or more. Such mixing leaves the exponent p unchanged only when it renormalizes the same multipole matrix element; if it opens a lower-multipole radiative amplitude, the asymptotic exponent is instead set by that lower-threshold-power channel. Isotope choice is thus a controlled knob on absolute observability, but not always on p alone. Third, embedding any of the transitions in Table I in a structured photonic reservoir replaces the free-space threshold by an engineered one. In general, if the reservoir produces $J(\omega) \sim |\omega - \omega_c|^s$ near a band edge, then $P(t) \sim t^{-2(s+1)}$; the exponent s is set by the engineered density of states, dimensionality, mode structure, and emitter position, not by a simple substitution $\omega \to |\omega - \omega_c|$ in the free-space law. This is the regime in which the present threshold-based reasoning may become experimentally relevant.

[1] A. Einstein, Physikalische Zeitschrift **18**, 121 (1917).
[2] V. Weisskopf and E. Wigner, Zeitschrift für Physik **63**, 54 (1930).
[3] C. Cohen-Tannoudji, J. Dupont-Roc, and G. Grynberg, *Atom–Photon Interactions* (Wiley, New York, 1992).
[4] L. A. Khalfin, Soviet Physics JETP **6**, 1053 (1958).
[5] L. Fonda, G. C. Ghirardi, and A. Rimini, Reports on Progress in Physics **41**, 587 (1978).
[6] S. R. Wilkinson, C. F. Bharucha, M. C. Fischer, K. W. Madison, P. R. Morrow, Q. Niu, B. Sundaram, and M. G. Raizen, Nature **387**, 575 (1997).
[7] M. C. Fischer, B. Gutiérrez-Medina, and M. G. Raizen, Physical Review Letters **87**, 040402 (2001).
[8] C. Rothe, S. I. Hintschich, and A. P. Monkman, Physical Review Letters **96**, 163601 (2006).
[9] A. Crespi, F. V. Pepe, P. Facchi, F. Sciarrino, P. Mataloni, H. Nakazato, S. Pascazio, and R. Osellame, Physical Review Letters **122**, 130401 (2019).
[10] A. Vukics, G. Kónya, and P. Domokos, Scientific Reports **11**, 16337 (2021).
[11] A. Stokes and A. Nazir, Nature Communications **10**, 499 (2019).
[12] O. Di Stefano, A. Settineri, V. Macrì, L. Garziano, R. Stassi, S. Savasta, and F. Nori, Nature Physics **15**, 803 (2019).
[13] A. Settineri, O. Di Stefano, D. Zueco, S. Hughes, S. Savasta, and F. Nori, Physical Review Research **3**, 023079 (2021).
[14] F. Giacosa, Multichannel decay law, Physics Letters B **831**, 137200 (2022).
[15] P. Facchi and S. Pascazio, Physics Letters A **241**, 139 (1998).
[16] F. Giacosa and K. Kyzioł, Acta Physica Polonica A **146**, 704 (2024).
[17] E. Lassalle, C. Champenois, B. Stout, V. Debierre, and T. Durt, Physical Review A **97**, 062122 (2018).
[18] H. E. Moses, Physical Review A **8**, 1710 (1973).
[19] J. Seke, Physica A **203**, 269 (1994).
[20] Lassalle *et al.* in fact reach the opposite ranking: for the monitored anti-Zeno problem, electric-dipole transitions are unobservable and forbidden lines are favored, exactly because the same threshold exponent enters the measurement-modified decay rate as $(\omega_X/\omega_0)^{s-1}$ rather than as the free-tail exponent.
[21] E. A. Power and S. Zienau, Philosophical Transactions of the Royal Society A **251**, 427 (1959).
[22] R. G. Woolley, Proceedings of the Royal Society A **321**, 557 (1971).
[23] W. E. Lamb, Physical Review **85**, 259 (1952).
[24] W. E. Lamb, R. R. Schlicher, and M. O. Scully, Physical Review A **36**, 2763 (1987).
[25] P. L. Knight and P. W. Milonni, Physics Letters A **56**, 275 (1976).
[26] N. A. Enaki, JETP **82**, 81 (1996).
[27] Y. Aharonov and C. K. Au, Physical Review A **20**, 2245 (1979).
[28] V. Debierre, T. Durt, A. Nicolet, and F. Zolla, Physical Review A **92**, 023825 (2015).
[29] R. M. Corless, G. H. Gonnet, D. E. G. Hare, D. J. Jeffrey, and D. E. Knuth, On the Lambert w function, Advances in Computational Mathematics **5**, 329 (1996).
[30] M. Block, O. Rehm, P. Seibert, and G. Werth, European Physical Journal D **7**, 461 (1999).
[31] V. Letchumanan, G. Wilpers, M. Roberts, S. A. Webster, M. Imai, G. P. Barwood, H. A. Klein, and P. Gill, Physical Review A **72**, 012509 (2005).
[32] M. Roberts, P. Taylor, G. P. Barwood, W. R. C. Rowley, and P. Gill, Physical Review A **62**, 020501(R) (2000).

Appendix A: Length-gauge

Here we show explicitly how the familiar electric-dipole coupling is related to the Coulomb-gauge matrix element used in the text. In the dipole approximation,

$$\langle g; 1_{k\lambda}|V_{\mathbf{A}\cdot\mathbf{p}}|e;0\rangle = \frac{e}{m_e}\mathcal{A}_k\,\boldsymbol{\epsilon}_{k\lambda}\cdot\mathbf{p}_{ge}. \tag{A1}$$

For atomic eigenstates, the momentum matrix element is fixed by the position matrix element. Since $[H_A, \hat{\mathbf{r}}] = -i\hbar\hat{\mathbf{p}}/m_e$,

$$\mathbf{p}_{ge} = im_e\omega_0\,\mathbf{r}_{ge}, \qquad \omega_0 = \frac{E_e - E_g}{\hbar}. \tag{A2}$$

Substituting this into (A1) gives

$$\langle g; 1_{k\lambda}|V_{\mathbf{A}\cdot\mathbf{p}}|e;0\rangle = ie\omega_0\mathcal{A}_k\,\boldsymbol{\epsilon}_{k\lambda}\cdot\mathbf{r}_{ge}. \tag{A3}$$

On the other hand, the transverse electric field of a single mode is $\hat{\mathbf{E}} = -\partial_t\hat{\mathbf{A}}$, so its one-photon amplitude is, up to an irrelevant phase,

$$\mathcal{E}_k = \omega_k\mathcal{A}_k. \tag{A4}$$

With the electric dipole operator $\mathbf{d} = -e\hat{\mathbf{r}}$, the length-gauge interaction $V_{\mathbf{d}\cdot\mathbf{E}} = -\mathbf{d}\cdot\mathbf{E}$ therefore gives

$$\langle g; 1_{k\lambda}|V_{\mathbf{d}\cdot\mathbf{E}}|e;0\rangle = e\omega_k\mathcal{A}_k\,\boldsymbol{\epsilon}_{k\lambda}\cdot\mathbf{r}_{ge} \tag{A5}$$

Up to phase. (A3) and (A5) agree at the physical emitted frequency $\omega_k = \omega_0$, so both gauges give the same golden-rule decay rate. Away from resonance, however, the Coulomb-gauge matrix element carries $\omega_0\mathcal{A}_k$ whereas the length-gauge one carries $\omega_k\mathcal{A}_k$; this is the origin of the different low-frequency powers discussed in the main text.

Appendix B: Eliminating the photon amplitudes

Here we derive (5). We insert the most general form of the time-evolved state

$$|\psi(t)\rangle = c_e(t)e^{-iE_e t/\hbar}|e;0\rangle + \sum_{k,\lambda} c_{k\lambda}(t)e^{-i(E_g+\hbar\omega_k)t/\hbar}|g;1_{k\lambda}\rangle \tag{B1}$$

into the Schrödinger equation with the rotating-wave interaction (3). Since $\omega_0 = (E_e - E_g)/\hbar$, the two amplitudes obey

$$\dot{c}_e(t) = -i\sum_{k,\lambda} g^*_{k\lambda}c_{k\lambda}(t)e^{-i(\omega_k-\omega_0)t}, \tag{B2}$$

$$\dot{c}_{k\lambda}(t) = -ig_{k\lambda}c_e(t)e^{+i(\omega_k-\omega_0)t}. \tag{B3}$$

The photon amplitudes vanish initially, $c_{k\lambda}(0) = 0$, so (B3) integrates to

$$c_{k\lambda}(t) = -ig_{k\lambda}\int_0^t dt'\, c_e(t')e^{+i(\omega_k-\omega_0)t'}. \tag{B4}$$

Substituting this expression into (B2) gives

$$\begin{aligned}\dot{c}_e(t) &= -\sum_{k,\lambda}|g_{k\lambda}|^2\int_0^t dt'\, e^{-i(\omega_k-\omega_0)(t-t')}c_e(t') \\ &= -\int_0^t dt'\, K(t-t')c_e(t'),\end{aligned} \tag{B5}$$

with

$$K(\tau) = \sum_{k,\lambda}|g_{k\lambda}|^2 e^{-i(\omega_k-\omega_0)\tau}. \tag{B6}$$

This is exact within the one-excitation, rotating-wave model. The continuum and Markov approximations enter only after this step.

Appendix C: Coulomb-gauge multipole coupling spectrum

We outline the derivation of (12). The Coulomb-gauge interaction between an atomic electron and the quantized electromagnetic field, without invoking the dipole approximation, is

$$V = \frac{e}{m_e}\sum_{\mathbf{k},\lambda}\mathcal{A}_k\left[a_{\mathbf{k}\lambda}\,\boldsymbol{\epsilon}_{\mathbf{k}\lambda}\cdot\hat{\mathbf{p}}\,e^{i\mathbf{k}\hat{\mathbf{r}}} + \text{h.c.}\right], \tag{C1}$$

with $\mathcal{A}_k = \sqrt{\hbar/(2\epsilon_0\omega_k V)}$. The multipole expansion of $e^{i\mathbf{k}\cdot\hat{\mathbf{r}}}$ in spherical harmonics gives, schematically,

$$\boldsymbol{\epsilon}_{\mathbf{k}\lambda}\cdot\hat{\mathbf{p}}\,e^{i\mathbf{k}\cdot\hat{\mathbf{r}}} \;\sim\; \sum_{L\geq 1}(kr)^{L-1}\,T^{(E)}_L \;+\; \sum_{L\geq 1}(kr)^{L}\,T^{(M)}_L, \tag{C2}$$

where $T^{(E)}_L$ and $T^{(M)}_L$ are dimensionless angular operators carrying the electric and magnetic multipole indices, respectively. The Lth electric multipole starts at order $(kr)^{L-1}$ because the leading term in the expansion is the E_1 dipole, and each additional multipole index requires one more spatial derivative. The magnetic multipole of order L carries one additional power of kr relative to the electric multipole of the same order because the magnetic moment couples to $\nabla\times\mathbf{A}$, which brings down an extra factor of k in matrix elements [3].

For a one-photon transition from $|e\rangle$ to $|g\rangle$ of pure multipole character (EL) or (ML), the matrix element of V between the initial state $|e;0\rangle$ and the final state $|g;1_{\mathbf{k}\lambda}\rangle$ is therefore

$$\hbar g_{\mathbf{k}\lambda} \;\propto\; \mathcal{A}_k\,k^{L-1+\delta_M}\,M_L, \tag{C3}$$

where $\delta_M = 0$ for electric and $\delta_M = 1$ for magnetic multipoles, and M_L is the reduced matrix element of the appropriate multipole operator between the atomic states. Squaring and using $\mathcal{A}_k^2 \propto 1/\omega_k$, $k = \omega_k/c$,

$$|g^{(EL)}_{\mathbf{k}\lambda}|^2 \propto \frac{1}{\omega_k}\cdot\omega_k^{2(L-1)} \;=\; \omega_k^{2L-3}, \tag{C4}$$

$$|g^{(ML)}_{\mathbf{k}\lambda}|^2 \propto \frac{1}{\omega_k}\cdot\omega_k^{2L} \;=\; \omega_k^{2L-1}. \tag{C5}$$

These are the multipole-resolved coupling scalings quoted in (12). Multiplying by the free-space photon density of states $\rho(\omega)\propto\omega^2$ and summing over polarizations gives

$$J_{EL}(\omega)\propto\omega^{2L-1}, \qquad J_{ML}(\omega)\propto\omega^{2L+1} \quad (\omega\to 0^+), \tag{C6}$$

matching (13). The full hydrogenic form factor of Moses [18] and Seke [19] adds an ultraviolet regulator of the form $[1+(\omega/\omega_X)^2]^{-\mu}$, where $\omega_X\sim c/a_0$ is the inverse Bohr time. This regulator controls the short-time (Zeno) physics and, more generally, is part of the smooth form factor $F(\omega)$ in Eq. (19). Only after the long-wavelength estimate $F(0)\simeq F(\omega_0) = 1$ does the coefficient reduce to the line-parameter form used in (20).

Appendix D: Origin of the threshold prefactor

We now derive the denominator used in (17). The memory equation (5) is most transparent after a Laplace transform,

$$\tilde{c}_e(s) \equiv \int_0^\infty dt\, e^{-st}c_e(t), \qquad \text{Re}\, s > 0. \tag{D1}$$

Using $c_e(0) = 1$, (5) gives

$$s\tilde{c}_e(s) - 1 = -\tilde{K}(s)\tilde{c}_e(s), \qquad \tilde{c}_e(s) = \frac{1}{s+\tilde{K}(s)}. \tag{D2}$$

The continuum kernel (6) has transform

$$\tilde{K}(s) = \int_0^\infty d\omega \, \frac{J(\omega)}{s + i(\omega - \omega_0)}. \tag{D3}$$

Thus every continuum frequency produces a singularity at $s_\omega = -i(\omega - \omega_0)$. The pole near $s = -\Gamma/2 - i\Delta$ gives the exponential part; the late-time correction comes from the branch cut produced by the continuum of s_ω values.

To isolate the threshold contribution, evaluate the discontinuity of $\tilde{c}_e(s)$ across this cut. Near the lower edge $\omega \simeq 0$, the point on the cut is far from the resonance pole: $|s_\omega| \simeq \omega_0$. In weak coupling, $|\tilde{K}(s_\omega)| \ll |s_\omega|$, so (D2) can be expanded as

$$\tilde{c}_e(s) = \frac{1}{s + \tilde{K}(s)} \simeq \frac{1}{s} - \frac{\tilde{K}(s)}{s^2} + \cdots . \tag{D4}$$

Only $\tilde{K}(s)$ has a discontinuity across the continuum cut. The first term $1/s$ has no threshold cut and therefore does not contribute to $c_{\rm cut}$. Using

$$\frac{1}{x + i0} - \frac{1}{x - i0} = -2\pi i \, \delta(x), \tag{D5}$$

(D3) gives, up to an overall phase convention that does not affect the magnitude,

$$\mathrm{Disc}\, \tilde{K}(s_\omega) \propto J(\omega). \tag{D6}$$

Therefore the discontinuity of the excited-state amplitude is

$$\mathrm{Disc}\, \tilde{c}_e(s_\omega) \simeq -\frac{\mathrm{Disc}\, \tilde{K}(s_\omega)}{|s_\omega|^2} \propto \frac{J(\omega)}{(\omega - \omega_0)^2}. \tag{D7}$$

This is the origin of the two off-resonant denominators. Equivalently, one denominator appears when the initially prepared excited amplitude couples into an off-resonant continuum mode, and the second appears when that continuum component is projected back onto the excited amplitude in the survival amplitude.

Inverting the Laplace transform along the cut then gives

$$c_{\rm cut}(t) \propto \int_0^\infty d\omega \, \frac{J(\omega)}{(\omega - \omega_0)^2} e^{-i(\omega - \omega_0)t}. \tag{D8}$$

Multiplying by the trivial phase convention used for $c_e(t)$ gives the equivalent form used in the main text, (17). Since the late-time integral is controlled by $\omega \simeq 0$, the denominator is smooth and may be replaced by ω_0^{-2} to leading order.